

# Feasible Space Monitoring for Multiple Control Barrier Functions with application to Large Scale Indoor Navigation

Hardik Parwana<sup>1</sup>, Mitchell Black<sup>2</sup>, Bardh Hoxha<sup>2</sup>, Hideki Okamoto<sup>2</sup>, Georgios Fainekos<sup>2</sup>,  
Danil Prokhorov<sup>2</sup>, Dimitra Panagou<sup>1,3</sup>

**Abstract**—Quadratic programs (QP) subject to multiple time-dependent control barrier function (CBF) based constraints have been used to design safety-critical controllers. However, ensuring the existence of a solution at all times to the QP subject to multiple CBF constraints is non-trivial. We quantify the feasible solution space of the QP in terms of its volume. We introduce a novel feasible space volume monitoring control barrier function that promotes compatibility of barrier functions and, hence, existence of a solution at all times. We show empirically that our approach not only enhances feasibility but also exhibits reduced sensitivity to changes in the hyperparameters such as gains of nominal controller. Finally, paired with a global planner, we evaluate our controller for navigation among humans in the AWS Hospital gazebo environment. The proposed controller is demonstrated to outperform the standard CBF-QP controller in maintaining feasibility.

## I. INTRODUCTION

*Videos accompanying examples and simulation results as well as a short description of our work can be seen at <https://www.youtube.com/watch?v=N94NqPKjRSM>.*

Designing a safety-critical robot motion stack for ensuring the satisfaction of multiple, possibly time-dependent, state and input constraints is an active area of research. This work deals with the formulation of low-level controllers for control-affine dynamical systems based on control barrier functions (CBFs). Given a constraint set, a CBF for given robot dynamics can be designed such that imposing a restriction on its rate-of-change in the control design guarantees constraint satisfaction for all times. This condition is typically imposed on the control input in an optimization problem such as a quadratic program (QP). In the presence of multiple constraint sets, it is common to simultaneously impose CBFs designed independently for each constraint in the controller. However, in such implementations, no guarantees for existence of a control satisfying all the CBF constraints exist, and violation of safety may result.

In this work, we analyze the conditions under which a controller with multiple CBF constraints admit a solution for all time, a property we call persistent feasibility. At a given state and time, we quantify the feasible control input space defined by CBF constraints and input bounds in terms of its volume, and introduce a novel feasible-space

control barrier function (FS-CBF) that restricts the rate-of-change of the volume of the feasible space. For control-affine dynamics and polytopic input constraints, this feasible space takes the form of a convex polytope. Existence of an FS-CBF is shown to be a necessary and sufficient condition for enforcing compatibility of multiple CBFs.

Two commonly used approaches are employed in the literature for handling multiple CBF constraints to tackle the feasibility problem: combining all barrier functions into a single one [1], [2], [3] or imposing the barriers simultaneously [4], [5], [6]. In [1], [3], barrier functions are combined into a single barrier constraint through a smoothed minimum (or maximum) operator. Employing non-smooth analysis, [2] constructs a barrier function with the non-smooth minimum (or maximum) operation. When multiple CBF constraints are imposed in a CBF-QP formulation, [4], [5] assumes compatibility and hence existence of a suitable control input. A constraint relaxation scheme is proposed in [6] whenever CBF-QP becomes infeasible, albeit without guarantees of safety.

A few studies explicitly try to circumvent the persistent feasibility issue. A sampling-and-grid refinement method is proposed in [7] to search the domain of state space over which multiple control barrier functions are compatible. However, it does not propose a controller to confine the robot to this domain. A sum-of-squares (SoS)-based CBF synthesis method when constraint sets are described by polynomial functions is given in [8]. In [9], sufficient conditions are provided for designing multiple CBFs concurrently so that a QP-based controller using all the CBFs will always be feasible. The work by [10] consolidates multiple CBFs into one CBF and proposes a predictor-corrector adaptation law for weights of constituent constraint functions. Additionally, a CBF learning framework is proposed in [11] for decentralized but cooperative multi-agent systems. Some works allow class- $\mathcal{K}$  functions to adapt by having time-varying parameters. The work by [12] creates a dataset of persistently feasible and eventually infeasible parameters by randomly sampling parameters and simulating the system forward. Adaptation of class- $\mathcal{K}$  parameters is also performed by posing CBF-QP as a differentiable layer in a predictor-corrector framework [13] and in learning paradigm [14] for learning of safe policies. Our motivation lies in ensuring safety in highly constrained indoor environments, such as in Fig. 1 with static as well as dynamically moving agents like humans. The decentralized nature of this problem and resulting large state space leads to prohibitive amount of

This work was mostly performed while Hardik Parwana was at Toyota.

<sup>1</sup> Department of Robotics, <sup>3</sup> Department of Aerospace Engineering, University of Michigan, Ann Arbor, USA {hardiksp, dpanagou}@umich.edu

<sup>2</sup> Toyota Motor North America, Research & Development, Ann Arbor, MI 48105, USA <first\_name.last\_name>@toyota.com.

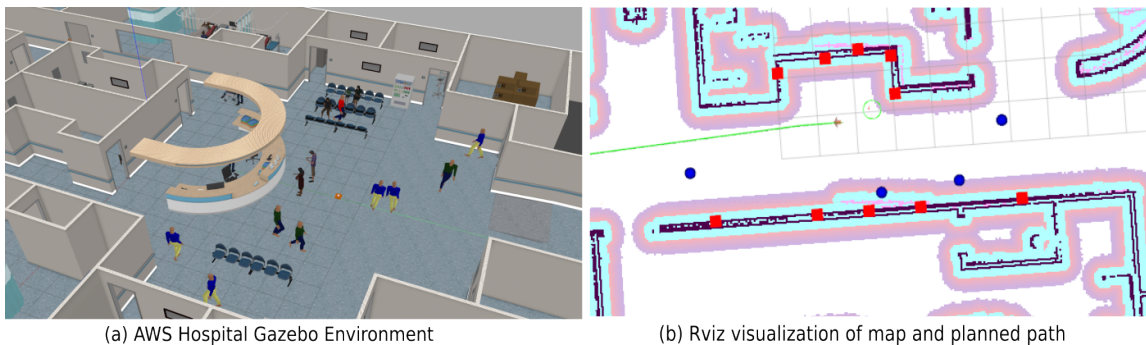


Fig. 1: Indoor navigation scenario. (a) Robot (green circle) navigating in AWS Hospital gazebo environment using proposed CBF controller. (b) Rviz visualization of the global map, global planner's path (green), humans (blue) and the nearest static obstacles (red, found in the way described in Section VI-B) used by the robot for collision avoidance.

possible scenarios thereby precluding synthesis of a valid CBFs akin to most of existing works.

With our FS-CBF, we provide a method to enforce compatibility between different CBF conditions. In cases where synthesis of our CBF is computationally feasible using any available algorithm, the existence of FS-CBF may be seen as complementing the existing literature. In other cases, we show through simulations that imposing feasible space volume as a candidate FS-CBF enhances persistent feasibility of standard CBF formulations, and additionally reduces sensitivity of CBF-QP controllers to hyperparameters such as gains of the nominal controller. This work, to the best of our knowledge, is the first to consider an optimization problem's feasible solution space volume and its gradient in control design. Previous approaches simply check if the CBF-QP is feasible, which amounts to checking whether the volume is non-zero or not. Finally, paired with ROS2 navigation stack planners, we also provide the first application of CBF-QP controller on a large scale indoor navigation scenario by implementing our controller on AWS Hospital environment in Gazebo [15].

#### Summary of Contributions:

- Introduced the notion of persistent feasibility and formulated Feasible-Space Control Barrier Function (FS-CBF) to quantify and restrict the rate-of-change of the volume of the feasible control input space.
- Demonstrated through simulations that FS-CBF enhances persistent feasibility and reduces hyperparameter sensitivity in CBF-QP controllers in a large scale indoor navigation scenario, integrated with ROS2 navigation stack planners.

In the subsequent, we formulate our problem in Section IV, introduce feasible space, methods to compute its volume, and design of FS-CBF in Section V. Finally, we present simulation results in Section VI.

## II. NOTATION

The set of real numbers is denoted as  $\mathbb{R}$ . The interior and boundary of a set  $\mathcal{C}$  is denoted by  $\text{Int}(\mathcal{C})$  and  $\partial\mathcal{C}$ . The empty set is denoted by  $\emptyset$ . For  $a \in \mathbb{R}^+$ , a continuous function  $\alpha : [0, a) \rightarrow [0, \infty)$  is a class- $\mathcal{K}$  function if it is strictly increasing and  $\alpha(0) = 0$ . For  $x \in \mathbb{R}, y \in \mathbb{R}^n$ ,  $|x|$  denotes

the absolute value of  $x$  and  $\|y\|$  denotes the  $L_2$  norm of  $y$ . The time derivative of  $x$  is denoted by  $\dot{x}$  and  $\frac{\partial F}{\partial x}$  denotes the gradient of a function  $F : \mathbb{R}^n \rightarrow \mathbb{R}$  with respect to  $x \in \mathbb{R}^n$ .

## III. SYSTEM DESCRIPTION

Consider a system with state  $x \in \mathcal{X} \subset \mathbb{R}^n$ , control input  $u \in \mathcal{U} \subset \mathbb{R}^m$  with the following dynamics

$$\dot{x} = f(x) + g(x)u, \quad (1)$$

where  $f : \mathcal{X} \rightarrow \mathbb{R}^n$  and  $g : \mathcal{X} \rightarrow \mathbb{R}^{n \times m}$  are locally Lipschitz continuous functions and  $x(t)$  is the solution of (1) at time  $t$  from initial condition  $x(0) = x_0$ . The set of allowable states  $\mathcal{S}(t)$ , hereby called safe set, at time  $t$  is specified as an intersection of  $N$  sets  $\mathcal{S}_i(t), i \in \{1, 2, \dots, N\}$ . Each  $\mathcal{S}_i(t)$  is defined as the 0-superlevel set of a continuously differentiable function  $h_i : \mathbb{R}^+ \times \mathcal{X} \rightarrow \mathbb{R}$ , i.e.,

$$\mathcal{S}_i(t) \triangleq \{x \in \mathcal{X} : h_i(t, x) \geq 0\}, \quad (2a)$$

$$\partial\mathcal{S}_i(t) \triangleq \{x \in \mathcal{X} : h_i(t, x) = 0\}, \quad (2b)$$

$$\text{Int}(\mathcal{S}_i(t)) \triangleq \{x \in \mathcal{X} : h_i(t, x) > 0\}. \quad (2c)$$

**Definition 1.** (Control Barrier Function) [16], [17] For the dynamical system (1),  $h_i : \mathbb{R}^+ \times \mathcal{X} \rightarrow \mathbb{R}$  is a control barrier function (CBF) on the set  $\mathcal{S}_i(t)$  defined by (2a)-(2c) if there exists an extended class- $\mathcal{K}$  function  $\alpha_i : \mathbb{R} \rightarrow \mathbb{R}^+$  and a set  $\mathcal{K}_i$  with  $\mathcal{S}_i \subseteq \mathcal{K}_i \subset \mathbb{R}^n$  such that  $\forall x \in \mathcal{K}_i, \forall t > 0$

$$\sup_{u \in \mathcal{U}} \left[ \frac{\partial h_i(t, x)}{\partial t} + L_f h_i(t, x) + L_g h_i(t, x)u \right] \geq -\alpha_i(h_i(t, x)) \quad (3)$$

It is assumed in this work that each  $h_i$  is a CBF for the set  $\mathcal{S}_i$  and that there exists a Lipschitz continuous controller  $u : \mathbb{R}^+ \times \mathcal{S}_i \rightarrow \mathcal{U}$  that satisfies (3), guaranteeing thus the forward invariance of the set  $\mathcal{S}_i$  under the closed-loop dynamics (1) [16], [17]. Finally, we review the following QP controller that is often used to enforce multiple CBF constraints

$$u(t, x) = \arg \min \|u - u_{ref}(t, x)\|^2 \quad (4)$$

$$\text{s.t. } \dot{h}_i(t, x) \geq \alpha_i(h_i(t, x)), i \in \{1, \dots, N\},$$

where  $u_{ref} : \mathbb{R}^+ \times \mathcal{X} \rightarrow \mathcal{U}$  is a reference control policy.

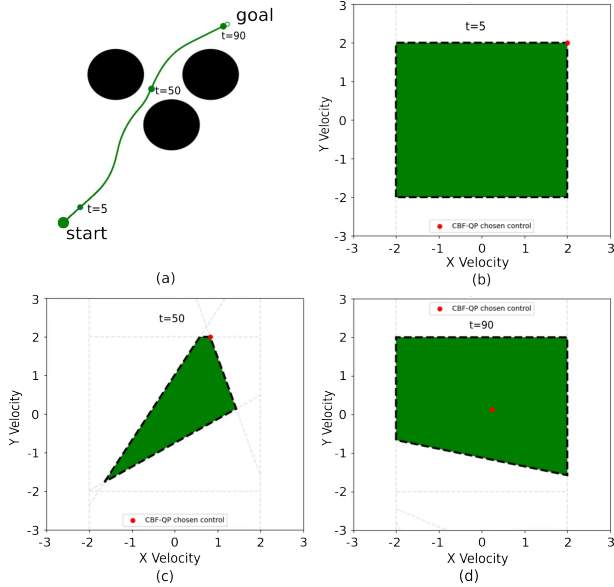


Fig. 2: Feasible space (green) of a single integrator agent with X, Y velocity inputs as it navigates to its goal location with  $N=3$  in (4) while avoiding obstacles (black). (a) The path in configuration space, (b), (c), (d) feasible control space visualization at different times. The dotted lines represent hyperplane equations that constrain the control input. The  $2 \times 2$  square is formed by control input bound. Other hyperplanes are formed as a result of CBF equations.

#### IV. PROBLEM FORMULATION

Given a barrier function  $h_i, i \in \{1, \dots, N\}$ , the set of control inputs that satisfy the CBF derivative constraint (4) for a given state  $x$  at time  $t$  are given by

$$\mathcal{U}_i(t, x) = \{u \in \mathbb{R}^m \mid \dot{h}_i(t, x, u) + \alpha_i(h_i(t, x)) \geq 0\}. \quad (5)$$

**Definition 2. Feasible CBF Space:** At a given time  $t$  and state  $x \in \mathcal{X}$ , the feasible CBF space  $\mathcal{U}_c \subset \mathbb{R}^m$  is the intersection of aforementioned sets with control input domain

$$\mathcal{U}_c(t, x) = \bigcap_{i=1}^N \mathcal{U}_i(t, x) \cap \mathcal{U}. \quad (6)$$

For control-affine dynamics, the constraints (5) are affine in  $u$  and represent halfspaces. If the input domain is polytopic, that is,  $\mathcal{U} = \{u \in \mathbb{R}^m \mid A_u u \leq b_u\}, A_u \in \mathbb{R}^{2m \times m}, b_u \in \mathbb{R}^{2m}$ , then the feasible space  $\mathcal{U}_c$  is a convex polytope. Figure 2 visualizes the polytope for a single integrator-modeled robot as it navigates around obstacles. For brevity, we will be denoting the feasible space in following form:

$$\mathcal{U}_c(t, x) = \{u \in \mathbb{R}^m \mid A(t, x)u \leq b(t, x)\} \quad (7)$$

where  $A : \mathbb{R}^+ \times \mathbb{R}^n \rightarrow \mathbb{R}^{(N+2m) \times m}, b : \mathbb{R}^+ \times \mathbb{R}^n \rightarrow \mathbb{R}^{(N+2m) \times 1}$ . We also denote each row of  $A$  by  $a_i$  and each element of  $b$  by  $b_i, i \in \{1, 2, \dots, N\}$ .

**Definition 3. (Persistently Feasible CBFs)** Given a Lipschitz continuous controller  $\pi : \mathcal{X} \rightarrow \mathcal{U}$ , the functions  $h_i$  are persistently feasible for dynamics (1) with  $u = \pi(x)$  in (1) if  $\exists E \subset \mathcal{X}$  such that  $\mathcal{U}_c(t, x) \neq \emptyset \forall t \geq 0, x_0 \in E$ .

We now describe our objective for persistent feasibility.

**Problem 1.** Consider the dynamical system (1) subject to  $N$  barrier function constraints  $h_i(t, x) \geq 0$  where each  $h_i$ , defined in (2), is a CBF with class- $\mathcal{K}$  function  $\alpha_i$  for the set  $\mathcal{S}_i$  respectively. If for the initial state  $x_0 \in \mathbb{R}^n, \mathcal{U}_c(0, x_0) \neq \emptyset$ , design a controller  $\pi$  that renders the CBFs  $h_i, i \in \{1, \dots, N\}$  persistently feasible, that is,  $\mathcal{U}_c(t, x) \neq \emptyset, \forall t > 0$ .

#### V. FEASIBLE VOLUME CONTROL BARRIER FUNCTION

The infeasibility of CBF-QP results when  $\mathcal{U}(t, x)$  becomes empty. In this section, we propose a novel control barrier function built upon the feasible space as a means to solving Problem 1. First, we provide some preliminaries on computing exact and approximate volume of convex polytopes and then present our formal results on FS-CBF.

##### A. Polytope Volume Estimation

A measure of the feasible space is its volume. Given a polytope  $P = \{Au \leq b\}$ , its volume is given by  $\text{vol}(P) = \int_P du$ . This integral does not admit an analytical expression in general and therefore cannot be used directly for control. Below we describe several ways to approximate the volume of feasible space.

1) *Monte Carlo:* A common approach to estimating polytope volume is to evaluate the integral with Monte Carlo (MC) sampling[18], [19]. This method is known to work well for low-dimensional spaces, but not for high-dimensional spaces[20]. Moreover, since Monte Carlo estimates are prone to be noisy, this method is also not suitable for evaluating gradients, which are needed to develop CBF conditions.

Below we describe two other approximate ways to compute the feasible space volume. It is worth mentioning that 2,3 are under-approximations, while MC can over- or under-approximate the feasible space volume depending on the samples.

2) *Chebyshev Ball of a Polytope:* The center  $c$  and radius  $r$  of the largest sphere contained inside a polytope, called Chebyshev ball, can be computed with the following Linear Program (LP)[21, Chapter 8]

$$\min_{c, r} \quad -r \quad (8a)$$

$$\text{s.t.} \quad a_i c + \|a_i\| r \leq b_i, \forall i \in \{1, 2, \dots, N\} \quad (8b)$$

3) *Inscribing Ellipsoid:* An ellipsoid  $E$  is an image of the unit ball under affine transformation  $(B, d), E = \{Bu + d \mid \|u\| \leq 1\}$  where  $B \in S_{++}^m$  and  $d \in \mathbb{R}^{m \times 1}$ . Using the fact that the ellipsoid volume is proportional to  $\det B$ , the maximum volume ellipsoid can be obtained by solving the following convex optimization problem [21, Chapter 8]

$$\min_{B, d} \quad \log \det B \quad (9a)$$

$$\text{s.t.} \quad \|Ba_i\| + a_i d \leq b_i, \forall i \in \{1, 2, \dots, N\} \quad (9b)$$

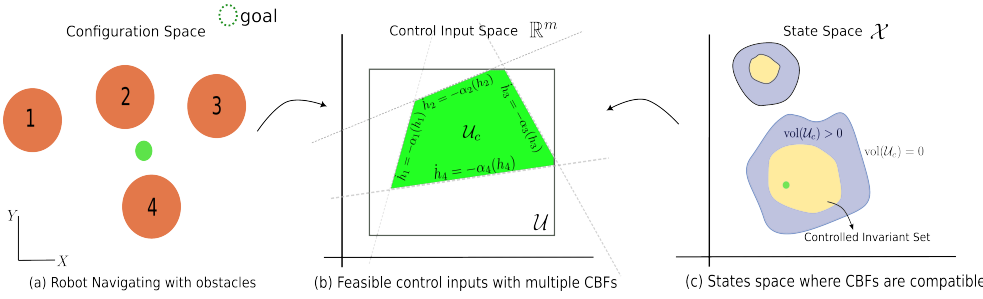


Fig. 3: (a) Configuration space of green robot with illustrative orange obstacles, (b) The feasible control space  $\mathcal{U}_c$  defined by multiple CBFs at the current state and time. Its volume is given by the area of the green region. (c) The state space domain (example) over which CBFs are compatible, i.e., volume of the polytope  $\mathcal{U}_c$  is  $> 0$ . The controlled invariant set is a subset of domain of compatibility that can actually be maintained forward invariant.

### B. Polytope Volume Gradients

Gradients over Monte Carlo estimate are prone to be noisy to the choice of random samples  $s_i$ . The sphere and ellipsoid on the other hand are computed using convex programs and, therefore, we can exploit sensitivity analysis [22] to compute the gradients of their volume w.r.t the polytope matrices  $A, b$ . Libraries like `cvxpy` [23] readily provide interface to differentiate through convex programs. However, we note that the volume of the polytope as well as its inscribing sphere and ellipsoid are non-differentiable quantities. Consider the scenario shown in Fig. 4. Suppose the hyperplanes H1-H4 are stationary and the H5 is free to move towards the origin, thereby decreasing enclosed volume, or away from the origin, having no effect on the enclosed volume. The point of non-differentiability for the circle or ellipsoid is when H6 is tangent to them. For the remainder of the paper, we make the following assumption and leave the non-smooth analysis to future work.

**Assumption 1.** The volume of the convex polytope (7) is differentiable w.r.t to its constituent matrices  $A, b$ .

**Remark 1.** In practice, we may encounter states at which the volume is non-differentiable w.r.t matrices  $A, b$ . `Cvxpy` returns heuristic gradient values at points of non-differentiability and we employ these in our implementations. In experiments, we did not observe any negative effects of this approximation, but a more formal non-smooth control theoretic analysis and consideration of generalized gradients, similar to non-smooth CBFs[2], [24] is left for future work.

### C. Polytope Volume barrier function

Let  $\mathcal{V}(t, x) = \text{vol}(\mathcal{U}_c)(t, x)$ . The compatible state space is defined as the set of states  $D(t) = \{x \in \mathcal{X} \mid \mathcal{V}(t, x) \geq 0\}$  and is visualized in Fig. 3. We then aim to find a CBF  $\mathcal{V}_c : \mathbb{R}^+ \times \mathbb{R}^n \rightarrow \mathbb{R}$ , with class- $\mathcal{K}$  function  $\alpha_{\mathcal{V}_c}$ , that renders  $D(t)$  forward invariant using, for example, the following controller

$$\begin{aligned} \pi(t, x) &= \arg \min_{u \in \mathcal{U}} \|u - u_{ref}(t, x)\|^2 \\ \text{s.t. } \dot{\mathcal{V}}_c(t, x, u) &\geq -\alpha_{\mathcal{V}_c}(\mathcal{V}(t, x)) \end{aligned} \quad (10)$$

**Assumption 2.** (Necessity of CBFs) For any controlled invariant set  $C \subset \mathcal{X}$  of the (1), there exists a continuously

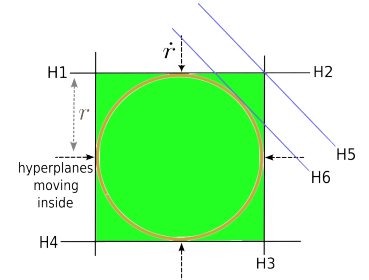


Fig. 4: Feasible space (green) of H1-H4 and its inscribing circle. H5 (H6) intersects the feasible space (circle) at a single point.

differentiable function  $h : \mathbb{R}^+ \times \mathcal{X} \rightarrow \mathbb{R}$  such that  $C$  is a 0-superlevel set of  $h$  and  $h$  is a CBF in sense of (1).

Under Assumption 2, the following theorem establishes the necessity and sufficiency of FS-CBF.

**Theorem 1.** Let  $h_i, i \in \{1, \dots, N\}$  be  $N$  barrier functions corresponding to  $N$  safe sets defined as in (2). Let  $\mathcal{V}(t, x)$  be the volume of the feasible CBF space  $\mathcal{U}_c(t, x)$  in the control domain defined in (6). Let  $D(t) = \{x \in \mathcal{X} \mid \mathcal{V}(t, x) \geq 0\}$  be the compatible state space of  $h_i, i \in \{1, \dots, N\}$ . Then under Assumption 2,  $h_i$  are persistently feasible iff there exists  $C \subset D$  and a function  $\mathcal{V}_c : \mathbb{R}^+ \times \mathbb{R}^n \rightarrow \mathbb{R}$  such that  $\mathcal{V}_c$  is a control barrier function on  $\mathbb{R}^+ \times C$  and  $x(0) \in C$ .

*Proof.* We prove the sufficiency first. Suppose that  $\mathcal{V}_c$  is a CBF with class- $\mathcal{K}$  function  $\alpha_{\mathcal{V}_c}$  on  $\mathbb{R}^+ \times C$ , with  $C \subset D$ . If  $x(0) \in C$ , then  $x(t) \in C, \forall t > 0$  under the action of the controller (10). Therefore,  $\mathcal{V}_c(t, x(t)) \geq 0, \forall t > 0$  and hence  $\mathcal{V}(t, x(t)) > 0$  for all  $t > 0$ , implying persistent feasibility.

Next, we show the necessity. Suppose  $h_i, i \in \{1, 2, \dots, N\}$  are persistently feasible. This implies that there exists a subset  $E \subset D$  that is control invariant. Existence of  $\mathcal{V}_c$  now trivially follows from Assumption 2.  $\square$

**Example 1.** We demonstrate a procedure to find a valid FS-CBF for navigating in the obstacle environment shown in Fig. 2. A Dubins car model is considered:  $\dot{x} = v \cos \theta, \dot{y} = v \sin \theta, \dot{\theta} = u$  where  $x, y$  are position,  $\theta$  is heading,  $v$  is fixed speed, and the angular velocity  $u \in [-0.5, 0.5]$  is the control input. We consider the constraint functions  $h_i = d_i^2 - d_{min}^2$ , with  $d_i$  being the distance to center of  $i^{th}$  obstacle and  $d_{min}$  the radius of obstacle. The compatible state space is thus given as the states  $x, y, \theta$  for which the feasible space (defined by the control input bounds and the corresponding Higher-Order CBF (HOCBF) constraints) is non-zero.  $\mathcal{U}_c(x)$  is visualized in Fig.5 for two different choices of linear class- $\mathcal{K}$  functions in the HOCBFs. To find the CBF corresponding to largest invariant set inside the compatible state space in Fig. 3(c), we use the refineCBF framework from [25] that leverages Hamilton-Jacobi (HJ) reachability analysis. A grid of  $201 \times 201 \times 81$  is used to discretize the state space in the domain  $x, y \in [0, 4], \theta \in [-\pi, \pi]$ , and a time horizon of

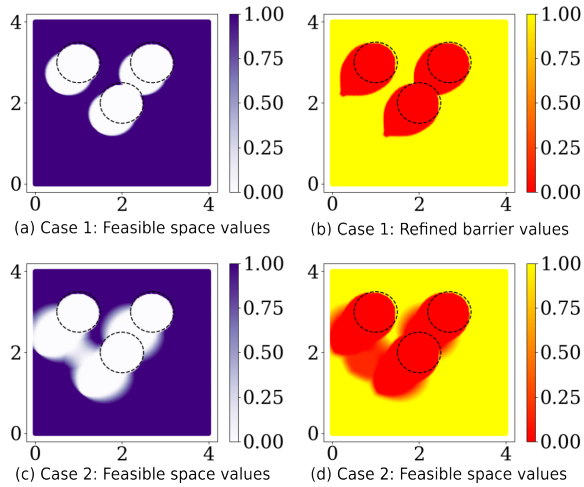


Fig. 5: Compatible space vs refined FS-CBF values at different  $X, Y$  and heading  $\theta = 45^\circ$ . (a),(c) Feasible space volume values for Case 1 - aggressive (a) and Case 2 - conservative (b) class- $\mathcal{K}$  function for HOCBF. (b), (d) refined CBF values. The compatible space (purple) is a subset of safe CBF space (yellow).

10 for computing the backward reachable sets. The feasible space volume is set to  $-1000$  whenever  $\min(h_1, h_2, h_3) < 0$ . The constructed FS-CBF space is shown in Fig. 5(b),(d). It is observed that the compatible state space is shrunk to remove states from where compatibility cannot be ensured in future with any controller.

Example 1 shows an application of an existing CBF synthesis method to construct  $\mathcal{V}_c$  for a simple system. For highly dynamic and constrained environments though, as previously mentioned, it is usually computationally prohibitive to consider all possible scenarios in the design of CBFs. Therefore, in practice, we assume  $\mathcal{V}_c = \mathcal{V}$  and use the controller (10) to enforce persistent feasibility.

**Remark 2.** We will demonstrate later in Section VI-A and Fig. 6 that imposing constraint (10) results in a control being chosen in the interior of feasible space of constraints (10), even when the nominal control input is outside the feasible space. This is done to prevent the volume from shrinking too fast. The controller (4) on the hand always chooses a point on boundary of feasible space. A mapping from  $u_{ref}$  to the interior of feasible space was also designed in [26] through a gauge map. The gauge map was designed in a different way than ours and focused on obtaining differentiable control design with a single barrier constraint only.

#### D. Valid class- $\mathcal{K}$ function for Feasible Space CBF

Finding a valid CBF entails simultaneously finding a barrier function  $h$  and a class- $\mathcal{K}$  function  $\alpha$  that satisfies the CBF derivative condition. While linear class- $\mathcal{K}$  functions are the first choice, below we show through two examples that the structure of the manifold defined by feasible space enclosed by a polytope can preclude the existence of such a function and propose a class- $\mathcal{K}$  function that it does admit. This analysis also provides insight into the nature of CBF-based controllers.

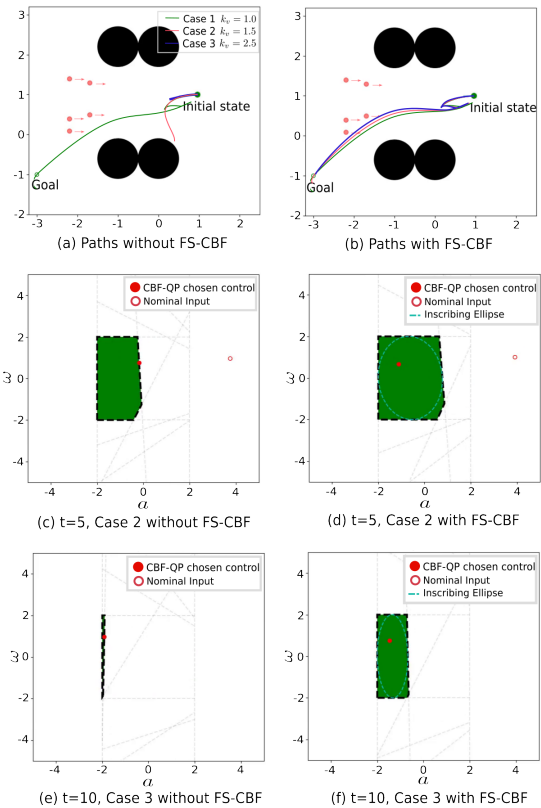


Fig. 6: Case study 1 - humans move towards the right. (a),(b) Paths for the three cases of  $k_v = 1, 1.5, 2.5$ . Blue and red paths in (a) end when CBF-QP becomes infeasible. (c), (d), (e), (f) Feasible space visualization with and without volume barrier function for  $k_v = 1.5$  in (c), (d) and  $k_v = 2.5$  in (e), (f). Note when nominal input is outside the feasible space, the volume barrier function maps it to interior of feasible space whereas CBF-QP (4) maps it to a point on the boundary.

**Example 2.** Consider a symmetric polygon of side length  $r$  in  $m$ -dimensional space, visualized in Fig. 3(d) for the 2D case. The volume of the polygon (or of its inscribing sphere) can easily be found to be  $k r^m$ , where  $k > 0$  depends on the dimension  $m$ . Suppose all the constituent hyperplanes move at a rate  $\dot{r}_v$  leading to a shrinking enclosed volume. Then, using  $r = (\mathcal{V}/k)^{1/m}$ , we have

$$\dot{\mathcal{V}} = kmr^{m-1}\dot{r} = km(k\mathcal{V})^{m-1/m}\dot{r}_v \quad (11)$$

where  $\dot{r}_v < 0$ . For the volume to be a CBF, we require a function  $\alpha$  such that

$$km\dot{r}(k\mathcal{V})^{m-1/m} \geq -\alpha(\mathcal{V}) \implies km|\dot{r}|(k\mathcal{V})^{m-1/m} \leq \alpha(\mathcal{V})$$

A linear class- $\mathcal{K}$  function cannot satisfy the above condition. A candidate function is  $\alpha(z) \propto (\mathcal{V})^{m-1/m}$ .

## VI. SIMULATION RESULTS

In this section, we present two case studies to evaluate the performance of the proposed volume barrier function.

### A. Case Study 1: Improving Feasibility and Sensitivity

This case study serves two purposes. First, we show that the addition of a feasible space volume barrier function enhances persistent feasibility. Second, it also helps reduce

sensitivity to the hyperparameters of the controller. Consider the scenario shown in Fig. 6 for a robot navigating to its goal location  $g$  while avoiding black prohibited zones and performing collision avoidance with humans. The robot is modeled as a dynamic unicycle with position  $p = [p_x, p_y]$ , velocity  $v$ , heading angle  $\psi$  and the following dynamics  $\dot{p}_x = v \cos \psi$ ,  $\dot{p}_y = v \sin \psi$ ,  $\dot{v} = a$ ,  $\dot{\psi} = \omega$ . The control inputs are the linear acceleration  $a$  and angular velocity  $\omega$ . The humans move with social force model [27][28], and consider the robot as one of the social agents. We consider the following reference (nominal) controller for the extended unicycle dynamics

$$\begin{aligned} \psi_{ref} &= \arctan\left(\frac{g_y - p_y}{g_x - p_x}\right), \quad \psi_e = \psi - \psi_{ref}, \quad \omega_{ref} = k_\omega \psi_e \\ v_{ref} &= k_x \|p - g\| \cos \psi_e, \quad a_{ref} = k_v (v - v_{ref}) \end{aligned} \quad (12)$$

where  $k_\omega, k_x, k_v > 0$  are user-chosen gains. We implement the CBF-QP (4) for three different values of the gain  $k_v$  to do sensitivity analysis. Cvxpylayers[23] is used to solve for the ellipse volume, and compute its gradient w.r.t polytope equations matrices  $A, b$ , and JAX’s autograd feature [29] is used to compute the gradient of  $A, b$  w.r.t states of the robot, humans, and the obstacles. We use JAX’s JIT feature to speed up computations whenever possible, and each control input computation takes 0.03 seconds. Fig. 6(a)-(b) show the trajectories of the robot, and Figs. 6(c)-6(e) show the variation of polytope volume under three different values of the gain  $k_v$ . We observe that when  $k_v$  is increased, that is, the nominal controller is more aggressive, the CBF-QP becomes infeasible sooner. Now, we impose the constraint that restricts the rate-of-change of the ellipse volume (10), computed using (9) as a CBF condition. Figs. 6(d), 6(f) show that the controller maintains feasibility, and the robot successfully reaches the goal. The visualization in Fig. 6 also shows that the nominal control input was not mapped to the boundary of the feasible set, but to its interior as mentioned in Remark 2. The video is available in supplementary material.

### B. Case Study 2: AWS Hospital

Next we evaluate our FS-CBF for navigating turtlebot3 robot in AWS Hospital gazebo environment shown in Fig. 1. We first generate a map of the environment without humans using ROS2 navigation stack. This map is used by global planner to plan paths, as well as by the CBF-QP controller to perform collision avoidance with static obstacles. At each time, the robot finds the closest occupied grid cell in the directions  $\theta = \beta 30^\circ, \beta \in \{1, 2, \dots, 12\}$ , and formulates 12 CBF constraints correspondingly. The humans are moved in real-time using a modified version of social force model plugin [30]. The position and velocity of humans is extracted from gazebo and made available to the robot, which then adds a CBF constraint for each human. The proposed FS CBF-QP is compared with CBF-QP in (4). The collision avoidance is enforced using distance as the higher-order barrier function of order two which is known to work well in the presence of a single constraint only. For obstacles,

we use linear class- $\mathcal{K}$  functions  $\alpha_1(h) = 2h, \alpha_2(h) = 6h$  for first and second-order HOCBF derivative conditions. For humans, we simulate two scenarios: scenario 1 uses  $\alpha_1(h) = 2h, \alpha_2(h) = 6h$  and scenario 2 uses  $\alpha_1(h) = h, \alpha_2(h) = 2h$ . Scenario 1 controller is therefore more aggressive than that of Scenario 2. For each scenario, the experiment is run 15 times, and the performance statistics are reported in Table I. In each run, the controller start time is changed within an interval of 2 seconds after humans start moving in the environment. The mean performance statistics are reported in Table I. The success rate is based on a robot rendered immobile after a hard collision in the gazebo. QP failures refer to the number of times the controller is infeasible over the run. Whenever the QP is infeasible, we implement the input from the previous time step. We see that FS-CBF-QP has better feasibility than CBF-QP. For the more aggressive scenario 1, the gains in feasibility are more pronounced compared to scenario 2. A video of the experiment is included in the supplementary material.

Method	Success Rate QP Failures		Success Rate QP Failures	
	Scenario 1		Scenario 2	
CBF-QP	0.91	54.2	1.0	16.85
FS CBF-QP	1.0	34.5	1.0	15.42

TABLE I: CBF-QP vs proposed FS-CBF-QP on gazebo

1) *Discussion of existing works:* Note that several existing approaches such as [31], [32], [33] for indoor navigation with humans rely only on fast replanning through a low-level planner based on simplified dynamics for collision avoidance, and do not employ a safety-critical controller. A direct comparison with these approaches is therefore impractical. Our controller is thus meant to complement existing planning frameworks by providing them with a controller capable of not only enforcing collision avoidance but arbitrary state constraints for control-affine robot dynamics. Among CBF-based approaches, [34] uses CBF-MPC, an MPC controller with constraints defined by CBF derivative conditions, for navigation in crowd, and [35] designs a novel CBF for polytopic obstacles and uses it in the CBF-MPC framework for navigation in corridor environments. From an application perspective, [34] does not consider indoor environments and [35] does not consider dynamic moving agents. While MPC does help with maintaining feasibility of CBF constraints, it is unlike our method of monitoring the volume of feasible space. Furthermore, since no guarantees of recursive feasibility of MPC have been shown to exist in dynamic indoor environments, these controllers are still prone to infeasibility. Consideration of the volume of feasible space defined by CBF constraints may complement these nonlinear optimization-based MPC methods in improving feasibility but this analysis is left for future work and here we focus only on CBF-QP formulations.

## VII. CONCLUSION

We propose a new barrier function that restricts the rate-of-change of the volume of feasible solution space of CBF-QP. We also provide empirical evaluation to corroborate our

theoretical results, and to show effectiveness in improving feasibility and in reducing sensitivity to changes in other system modules such as nominal controller. Future work will involve performing experiments with robots and non-smooth control theoretic analysis of FS-CBF.

## REFERENCES

- [1] D. Panagou, D. M. Stipanović, and P. G. Voulgaris, “Multi-objective control for multi-agent systems using Lyapunov-like barrier functions,” in *52nd IEEE Conference on Decision and Control*. IEEE, 2013, pp. 1478–1483.
- [2] P. Glotfelter, J. Cortés, and M. Egerstedt, “Nonsmooth barrier functions with applications to multi-robot systems,” *IEEE control systems letters*, vol. 1, no. 2, pp. 310–315, 2017.
- [3] D. M. Stipanović, C. J. Tomlin, and G. Leitmann, “Monotone approximations of minimum and maximum functions and multi-objective problems,” *Applied Mathematics & Optimization*, vol. 66, no. 3, pp. 455–473, 2012.
- [4] J. Usevitch, K. Garg, and D. Panagou, “Strong invariance using control barrier functions: A clark tangent cone approach,” in *2020 59th IEEE Conference on Decision and Control*. IEEE, 2020, pp. 2044–2049.
- [5] M. Aali and J. Liu, “Multiple control barrier functions: An application to reactive obstacle avoidance for a multi-steering tractor-trailer system,” in *2022 IEEE 61st Conference on Decision and Control (CDC)*. IEEE, 2022, pp. 6993–6998.
- [6] X. Wang, “Ensuring safety of learning-based motion planners using control barrier functions,” *IEEE Robotics and Automation Letters*, vol. 7, no. 2, pp. 4773–4780, 2022.
- [7] X. Tan and D. V. Dimarogonas, “Compatibility checking of multiple control barrier functions for input constrained systems,” in *2022 IEEE 61st Conference on Decision and Control (CDC)*. IEEE, 2022, pp. 939–944.
- [8] A. Clark, “Verification and synthesis of control barrier functions,” in *2021 60th IEEE Conference on Decision and Control (CDC)*. IEEE, 2021, pp. 6105–6112.
- [9] J. Breeden and D. Panagou, “Compositions of multiple control barrier functions under input constraints,” in *2023 American Control Conference (ACC)*. IEEE, 2023, pp. 3688–3695.
- [10] M. Black and D. Panagou, “Consolidated control barrier functions: Synthesis and online verification via adaptation under input constraints,” *arXiv preprint arXiv:2304.01815*, 2023.
- [11] Z. Qin, K. Zhang, Y. Chen, J. Chen, and C. Fan, “Learning safe multi-agent control with decentralized neural barrier certificates,” *arXiv preprint arXiv:2101.05436*, 2021.
- [12] W. Xiao, C. A. Belta, and C. G. Cassandras, “Feasibility-guided learning for constrained optimal control problems,” in *2020 59th IEEE Conference on Decision and Control (CDC)*. IEEE, 2020, pp. 1896–1901.
- [13] H. Parwana and D. Panagou, “Recursive feasibility guided optimal parameter adaptation of differential convex optimization policies for safety-critical systems,” in *2022 International Conference on Robotics and Automation (ICRA)*. IEEE, 2022, pp. 6807–6813.
- [14] W. Xiao, T.-H. Wang, R. Hasani, M. Chahine, A. Amini, X. Li, and D. Rus, “Barriernet: Differentiable control barrier functions for learning of safe robot control,” *IEEE Transactions on Robotics*, 2023.
- [15] [Online]. Available: <https://github.com/aws-robotics/aws-robomaker-hospital-world>
- [16] A. D. Ames, X. Xu, J. W. Grizzle, and P. Tabuada, “Control barrier function based quadratic programs for safety critical systems,” *IEEE Transactions on Automatic Control*, vol. 62, no. 8, pp. 3861–3876, 2016.
- [17] L. Lindemann and D. V. Dimarogonas, “Control barrier functions for signal temporal logic tasks,” *IEEE control systems letters*, vol. 3, no. 1, pp. 96–101, 2018.
- [18] Y. T. Lee and S. S. Vempala, “Convergence rate of riemannian hamiltonian monte carlo and faster polytope volume computation,” in *Proceedings of the 50th Annual ACM SIGACT Symposium on Theory of Computing*, 2018, pp. 1115–1121.
- [19] I. Z. Emiris and V. Fisikopoulos, “Practical polytope volume approximation,” *ACM Transactions on Mathematical Software (TOMS)*, vol. 44, no. 4, pp. 1–21, 2018.
- [20] [Online]. Available: <https://volesti.readthedocs.io/en/latest/tutorials/general.html>
- [21] S. P. Boyd and L. Vandenberghe, *Convex optimization*. Cambridge university press, 2004.
- [22] A. Agrawal, B. Amos, S. Barratt, S. Boyd, S. Diamond, and J. Z. Kolter, “Differentiable convex optimization layers,” *Advances in neural information processing systems*, vol. 32, 2019.
- [23] S. Diamond and S. Boyd, “Cvxpy: A python-embedded modeling language for convex optimization,” *The Journal of Machine Learning Research*, vol. 17, no. 1, pp. 2909–2913, 2016.
- [24] A. Thirugnanam, J. Zeng, and K. Sreenath, “Nonsmooth control barrier functions for obstacle avoidance between convex regions,” *arXiv preprint arXiv:2306.13259*, 2023.
- [25] S. Tonkens and S. Herbert, “Refining control barrier functions through hamilton-jacobi reachability,” in *2022 IEEE/RSJ International Conference on Intelligent Robots and Systems (IROS)*. IEEE, 2022, pp. 13 355–13 362.
- [26] S. Yang, S. Chen, V. M. Preciado, and R. Mangharam, “Differentiable safe controller design through control barrier functions,” *IEEE Control Systems Letters*, vol. 7, pp. 1207–1212, 2022.
- [27] D. Helbing and P. Molnar, “Social force model for pedestrian dynamics,” *Physical review E*, vol. 51, no. 5, p. 4282, 1995.
- [28] [Online]. Available: <https://pypi.org/project/socialforce/>
- [29] J. Bradbury, R. Frostig, P. Hawkins, M. J. Johnson, C. Leary, D. Maclaurin, G. Necula, A. Paszke, J. VanderPlas, S. Wanderman-Milne, and Q. Zhang, “JAX: composable transformations of Python+NumPy programs,” 2018. [Online]. Available: <http://github.com/google/jax>
- [30] [Online]. Available: [https://github.com/robotics-upo/gazebo.sfm\\_plugin](https://github.com/robotics-upo/gazebo.sfm_plugin)
- [31] S. Silva, N. Verdezoto, D. Paillacho, S. Millan-Norman, and J. D. Hernández, “Online social robot navigation in indoor, large and crowded environments,” in *2023 IEEE International Conference on Robotics and Automation (ICRA)*. IEEE, 2023, pp. 9749–9756.
- [32] P. Patompak, S. Jeong, N. Y. Chong, and I. Nilkhamhang, “Mobile robot navigation for human-robot social interaction,” in *2016 16th international conference on control, automation and systems (ICCAS)*. IEEE, 2016, pp. 1298–1303.
- [33] K. Cai, W. Chen, D. Dugas, R. Siegwart, and J. J. Chung, “Sampling-based path planning in highly dynamic and crowded pedestrian flow,” *IEEE Transactions on Intelligent Transportation Systems*, 2023.
- [34] V. Vulcano, S. G. Tarantos, P. Ferrari, and G. Oriolo, “Safe robot navigation in a crowd combining mpc and control barrier functions,” in *2022 IEEE 61st Conference on Decision and Control (CDC)*. IEEE, 2022, pp. 3321–3328.
- [35] A. Thirugnanam, J. Zeng, and K. Sreenath, “Safety-critical control and planning for obstacle avoidance between polytopes with control barrier functions,” in *2022 International Conference on Robotics and Automation (ICRA)*. IEEE, 2022, pp. 286–292.